

Dark matter searches going bananas: the contribution of Potassium (and Chlorine) to the 3.5 keV line

Tesla Jeltema^{1*} and Stefano Profumo^{1†}

¹*Department of Physics and Santa Cruz Institute for Particle Physics University of California, Santa Cruz, CA 95064, USA*

6 December 2024

ABSTRACT

We examine the claimed excess X-ray line emission near 3.5 keV with a new analysis of *XMM-Newton* observations of the Milky Way center and with a re-analysis of the data on M 31 and clusters. In no case do we find conclusive evidence for an excess. We show that known plasma lines, including in particular K XVIII lines at 3.48 and 3.52 keV, provide a satisfactory fit to the *XMM* data from the Galactic center. We assess the expected flux for the K XVIII lines and find that the measured line flux falls squarely within the predicted range based on the brightness of other well-measured lines in the energy range of interest. We then re-evaluate the evidence for excess emission from clusters of galaxies, including a previously unaccounted for Cl XVII line at 3.51 keV, and allowing for systematic uncertainty in the expected flux from known plasma lines and for additional uncertainty due to potential variation in the abundances of different elements. We find that no conclusive excess line emission is present within the systematic uncertainties in Perseus or in other clusters. Finally, we re-analyze *XMM* data for M 31 and find no statistically significant line emission near 3.5 keV to a level greater than one sigma.

Key words: dark matter – line: identification – Galaxy: centre – X-rays: galaxies – X-rays: galaxies: clusters

1 INTRODUCTION

The particle nature of the dark matter, comprising most of the gravitationally bound structures in the universe, is unknown. A far-ranging experimental and observational program is in place to search for non-gravitational signals that could point to a given class of particle dark matter candidates. While weakly interacting massive particles have attracted much attention, other particle candidates remain theoretically robust and observationally viable. Among such candidates, “sterile” neutrinos offer the appealing possibility of tying the dark matter problem to the issue of generating a mass for the Standard Model “active” neutrinos, provide an interesting warm dark matter candidate, and can be potentially associated with a mechanism to explain the baryon-antibaryon asymmetry in the universe (see Boyarsky et al. 2009, for a recent review).

Sterile neutrinos can mix with active neutrinos, and decay, on timescales much longer than the age of the Universe, to the two-body final state given by an active neutrino and a photon. The details of such process depend on the particular extension to the Standard Model that accommodates the sterile neutrino(s) (see e.g. Pal & Wolfenstein 1982), but the lifetime is set by a model-independent combination of the sterile-active neutrino mixing an-

gle θ and of the sterile neutrino mass m_s of the form

$$\tau \simeq 7.2 \times 10^{29} \text{ sec} \left(\frac{10^{-4}}{\sin(2\theta)} \right)^2 \left(\frac{1 \text{ keV}}{m_s} \right)^5. \quad (1)$$

Such a decay mode produces an almost monochromatic photon signal at an energy approximately equal to half the sterile neutrino mass. Cosmological production mechanisms and constraints from phase-space density restrict the relevant range for the sterile neutrino mass to, roughly, 0.5 – 100 keV (Boyarsky et al. 2009). As a result, the expected line from sterile neutrino two-body decays falls in the X-ray range.

Earlier this year, Bulbul et al. (2014) claimed the existence of an unidentified emission line at $E = (3.55 - 3.57) \pm 0.03$ keV from stacked *XMM-Newton* observations of 73 galaxy clusters with redshift ranging between 0.01 and 0.35. The line is observed with statistical significance greater than 3σ in three separate subsamples: (i) the individual Perseus cluster; (ii) combined data for the Coma, Centaurus and Ophiuchus clusters; (iii) all stacked 73 clusters in the sample. Chandra observations of Perseus indicate a line feature compatible with the *XMM* results; The line was not, however, observed in the Virgo cluster with Chandra data. Bulbul et al. (2014) explored possible contaminations from metal lines, notably from K and Ar, which would require however typical fluxes factors of 10-30 larger than predicted.

Shortly after the analysis of Bulbul et al. (2014), a 3.5 keV line was reported from *XMM-Newton* observations of both the

* tesla@ucsc.edu

† profumo@ucsc.edu

Perseus cluster and the Andromeda galaxy (M 31), while not being observed in “blank sky” observations (Boyarsky et al. 2014). The line intensity is compatible with a sterile neutrino with a mass of 7.06 ± 0.05 keV, and a mixing angle $\sin^2(2\theta) = (2.2-20) \times 10^{-11}$ (Boyarsky et al. 2014), compatible with the results of Bulbul et al. (2014), which quote a mass of about 7.1 keV and a mixing angle $\sin^2(2\theta) \sim 7 \times 10^{-11}$.

Considerable excitement from the model-building community followed the observations described above. Several studies focused on the possibility of decaying sterile neutrinos, and especially on the question of the genesis of the right abundance of such particles in the early universe and on the issue of how to embed such models in extensions to the Standard Model of particle physics (Ishida et al. 2014; Abazajian 2014; Baek & Okada 2014; Tsuyuki 2014; Allahverdi et al. 2014; Okada 2014; Modak 2014; Cline et al. 2014; Rosner 2014; Robinson & Tsai 2014; Abada et al. 2014; Okada & Orikasa 2014; Rodejohann & Zhang 2014; Haba et al. 2014). Other studies considered alternative possibilities, including exciting dark matter (Finkbeiner & Weiner 2014; Okada & Toma 2014), axion and axion-like dark matter (Higaki et al. 2014; Jaeckel et al. 2014; Lee et al. 2014; Cicoli et al. 2014; Ringwald 2014), axino dark matter (Kong et al. 2014; Choi & Seto 2014; Dias et al. 2014; Liew 2014; Conlon & Day 2014), gravitino dark matter (Bomark & Roszkowski 2014; Demidov & Gorbunov 2014), decaying moduli (Nakayama et al. 2014) or WIMPs (Chiang & Yamada 2014), light vector bosons (Shuve & Yavin 2014), R-parity violating (Kolda & Unwin 2014) or R-parity conserving (Dutta et al. 2014; Baer et al. 2014) decays of sparticles in supersymmetry, Majoron dark matter (Queiroz & Sinha 2014), magnetic dark matter (Lee 2014), dark transition electric dipoles (Geng et al. 2014), non-abelian dark matter models (Cline & Frey 2014), or effective theory constructions (Krall et al. 2014) (see also Frandsen et al. 2014, for a general model-building discussion). The possibility of dark matter pair-annihilation was also entertained in Dudas et al. (2014) and Baek et al. (2014).

More recently, Riemer-Sorensen (2014) used Chandra observations of the Milky Way center to probe the possibility that the 3.5 keV line originates from dark matter decay. No evidence was found for excess X-ray line emission in the energy of interest when including lines at the energies of known plasma lines. When including known emission lines, Riemer-Sorensen (2014) rules out at the 95% confidence level a dark matter decay scenario as the origin of the line signal reported by Bulbul et al. (2014) and Boyarsky et al. (2014). However, as this paper does not quote measured fluxes for the plasma emission lines near 3.5 keV, it is unclear if these are consistent with what is expected or could instead artificially mask a dark matter signal.

While the results of Riemer-Sorensen (2014), with the above caveat, put significant pressure on a dark matter decaying interpretation of the X-ray line observed from Galaxy clusters, Conlon & Powell (2014) point out that the magnetic field structure of the Milky Way is such that an axion-like particle conversion to a monochromatic X-ray photon in the presence of magnetic fields would still be a viable option. Conlon & Day (2014), in fact, found that for such a case the line intensity predicted, for instance, for M31 is two orders of magnitude larger than for the Milky Way.

In the present study we utilize *XMM-Newton* observations of the Milky Way center and of M31 with the purpose of testing a “new physics” origin for the 3.5 keV line reported by Bulbul et al. (2014) and Boyarsky et al. (2014). We illustrate that known plasma emission lines, with reasonable emissivities, provide a highly satisfactory fit to the Galactic center X-ray spectrum in the energy

range of interest (sec. 2.2) and we outline the implications for a dark matter interpretation of the 3.5 keV line, including obtaining the most stringent constraints on the dark matter lifetime for the corresponding ~ 7 keV mass (sec. 2.3); we then show that accounting for systematic uncertainties in the plasma emission line brightness in clusters of galaxies from both relative elemental abundances and temperature fully explains the 3.5 keV feature observed in three different systems and stacked systems of clusters of galaxies (sec. 3.1); finally, no statistical evidence to a level greater than one sigma is found for the existence of a 3.5 keV line from M 31 in a reanalysis of the *XMM* data. (sec. 3.2). We discuss our findings and conclude in sec. 4.

2 SEARCHING FOR DARK MATTER DECAY FROM THE MILKY WAY CENTER

As a starting point to our analysis, we focus on *XMM* observations of the Galactic center. The center of the Milky Way is an obvious target to search for non-gravitational signals from particle dark matter, such as photons from dark matter pair annihilation or decay. While astrophysical background emission, including significant flaring activity, is present in the region, simple estimates of the integrated line of sight density of dark matter within angular regions of the size of the field of view of X-ray instruments indicate that the Galactic center is likely the brightest direction in the sky for dark matter decay into photons. Here, we improve on a recent analysis that utilized *Chandra* X-ray observations of the Galactic center Riemer-Sorensen (2014) by employing archival public *XMM* observations, with a larger field-of-view, a higher effective area, and with a total cleaned exposure time a factor almost 2.5 greater than in the analysis of Riemer-Sorensen (2014). We also explore in detail the expected contribution of known plasma lines and whether these can self-consistently explain the observed emission.

2.1 *XMM* Data Analysis

In this section, we describe the observations we employed in our analysis, the data reduction, and the selection procedure. We initially considered all *XMM* observations pointed within $4'$ of the Galactic center and with exposure times of at least 10 ksecs. The EPIC MOS and PN data for all observations were reduced with the *XMM* SAS (version 13.5.0) software¹ using standard reduction techniques. The level 1 event files were reprocessed with the *emchain* and *epchain* tasks. Flare filtering, point source detection, and spectral extraction were carried out using the *XMM* ESAS package (Snowden et al. 2008; Kuntz & Snowden 2008). The lightcurve filtering tasks *mos-filter* and *pn-filter* within ESAS are designed to eliminate periods with elevated particle background. Filtering was accomplished by creating a histogram of the count rate in 60 second bins; a Gaussian was fit to the histogram, and periods when the count rate deviated by more than 1.5σ from the Gaussian peak were removed.

In the case of the Galactic center, Sgr A* is known to be highly variable, and, in addition to actual particle background flares, flaring activity of Sgr A* can also significantly change the observed count rate. In principle, flaring of Sgr A* should have no effect on our analysis, since it would not affect the flux of a dark-matter-induced line. However, these flares do significantly increase the

¹ <http://xmm.esac.esa.int/sas/>

obsID	MOS1 (ksec)	MOS2 (ksec)	PN (ksec)
0111350101	41.5	41.2	34.6
0202670701	79.9	83.4	53.6
0554750401	31.7	33.3	26.1
0604301001	39.2	41.2	20.9
0674601101	10.6	10.9	9.4
0202670801	93.3	97.0	62.5
0554750501	40.6	40.6	31.6
0658600101	47.1	47.6	39.8
0554750601	36.3	36.3	24.8
0658600201	39.7	42.7	32.6
0604300601	30.7	32.2	21.0
0112972101	21.3	21.3	16.9
0604300701	36.6	42.1	19.9
0604300801	34.6	34.6	27.6
0674600801	18.0	18.4	13.8
0604300901	20.9	22.1	13.5
0674601001	20.6	21.1	15.5
0202670601	32.2	34.8	22.4

Table 1. *XMM* obsID numbers and flare-filtered exposure times for the three EPIC cameras for the Galactic center observations used in our analysis.

background to line detection, as well as changing the spectral shape of Sgr A* (e.g. Nowak et al. 2012). We thus removed from our analysis observations during time periods with strong Sgr A* flares (October 3, 2002; April 2-5, 2007) as well as additional observations which were found to be very highly contaminated by variability and/or particle background flares. The observations utilized in our analysis and the remaining good exposure time after flare filtering for each instrument are catalogued in Table 1. The total flare-filtered exposure times are 675 ks, 700 ks, and 487 ks for the MOS1, MOS2, and PN detectors, respectively. Collectively, this exposure time is approximately 2.5 times larger than the *Chandra* observations used in the analysis of Riemer-Sørensen (2014).

Bright point sources were detected and masked using the ESAS task *cheese*, run on broad band images (0.4-7.2 keV), including a $\sim 20''$ region around Sgr A*; *cheese* also masks low-exposure regions of the detector like chip gaps and bad columns. We then extracted spectra from the full field-of-view for each detector, excluding CCD 6 on MOS1 which suffered micrometeoroid damage in March 2005, and corresponding redistribution matrix files (RMFs) and ancillary response files (ARFs) using the ESAS tasks *mos-spectra* and *pn-spectra*. No background spectra were created, as we choose to model the background rather than subtract it off. The individual spectra were then summed using the *mathpha* tool from the *FTOOLS* package (Blackburn 1995). Combined RMF and ARF files were generated using the *addrmf* and *addarf* routines in *FTOOLS*, weighted by the relative contribution of each observation to the total exposure time. Spectra and responses from the two MOS detectors were co-added to create a single combined MOS spectrum, while spectra and responses extracted from the PN detector were summed separately.

The stacked MOS and PN spectra were fit with *XSPEC* (version 12.8.1p, Arnaud 1996). The X-ray emission from the Galactic center region within the *XMM* field-of-view (radius of $\sim 15'$) is a complicated combination of numerous sources, including active stars, cataclysmic variables, low and high-mass X-ray binaries, supernova remnants, thermal gas, particle and instrumental backgrounds. As we are primarily interested here in determining if excess line emission is present around 3.5 keV, we did not attempt to fit a physically meaningful spectral model that accounts for all of

these components. Instead, we focused on obtaining a good fit to the continuum emission in the spectral range of interest. Specifically, we fit a narrow energy range from 3.0-4.5 keV. This energy range is large enough to be much broader than the energy resolution of the detectors (~ 100 eV) as well as containing several strong plasma emission lines based on which we can estimate the flux of weaker lines; at the same time, the energy window is small enough that we obtained a good fit with a simple power-law continuum plus astrophysical line emission.

We began by fitting the spectra to a simple power law plus a series of Gaussian lines, starting with the most significant plasma emission lines in the energy range taken from the *AtomDB* database² (Smith et al. 2001). We then successively added Gaussians for weaker plasma lines. Line energies were allowed to vary by ± 10 eV to account for uncertainty in the energy calibration of the detectors and in the atomic database. Known lines which improved the reduced χ^2 were kept, while those that did not improve the fit and had very low normalizations were removed. The lines included in the final fit (and the corresponding energies) were: S XVI (3.11 keV, 3.36 keV), Ar XVII (3.13 keV, 3.62 keV, 3.69 keV, 3.79 keV, 4.0 keV), Ar XVIII (3.32 keV), K XVIII (3.48, 3.52), Ca XIX (3.86, 3.90), Ca XX (4.11 keV). The resulting model yielded a very good fit to the data, with a reduced χ^2 of 0.98 ($\chi^2 = 267/273$ degrees of freedom) for the combined PN spectrum and a reduced χ^2 of 1.03 ($\chi^2 = 279/271$ degrees of freedom) for the combined MOS spectrum. The best fit and residuals are shown in Figure 1, which illustrates that no additional excess line is present in the data beyond the lines listed above.

Note that there are two plasma lines due to K XVIII right around 3.5 keV. Excluding these lines would significantly worsen the fit. Clearly, it is of paramount importance to assess the expected strength of these plasma lines, as underestimating their strength could mimic a dark matter signal, while overestimating it could hide a true dark matter line. In the following section, we take a similar approach to Bulbul et al. (2014) by taking the measured strength of several strong plasma lines near 3.5 keV and using these to estimate the strength of K XVIII emission. Notice that there is also a

² <http://www.atomdb.org/Webguide/webguide.php>

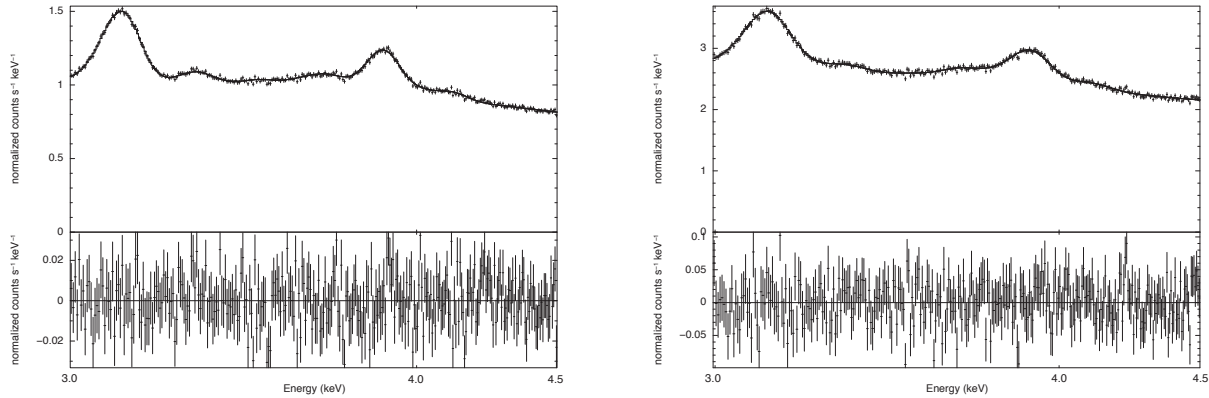


Figure 1. Stacked spectra of the Galactic center in the 3.0 to 4.5 keV band for the combined MOS (left) and PN (right) observations. Also shown are the best-fit model and residuals.

pair of lines from Cl XVII at 3.51 keV which are expected to contribute comparable flux to K XVIII for higher temperature plasmas ($kT \geq 5$ keV). These lines were not included in the analysis of Bulbul et al. (2014), but we include here their estimated contribution for temperatures of 5 keV or higher.

2.2 Predicting the Flux of the K XVIII Lines

We list the measured fluxes of several strong emission lines in the spectral energy range under scrutiny, as well as the sum of the two K XVIII lines, in Table 2. When predicting emissivities, each of these lines is considered as the sum of all closely spaced, significant lines which are unresolvable at the instrumental energy resolution. The lines/line complexes considered are: S XVI (2.620+2.623 keV), Ar XVII (3.124+3.126+3.140 keV), K XVIII (3.476+3.515 keV), Ar XVII (3.685 keV), Ca XIX (3.861+3.883+3.888+3.902 keV), and Ca XX (4.100+4.107 keV). We include the measured flux of S XVI for comparison to Bulbul et al. (2014), though it falls slightly outside our initial energy range. Note that we include the K XVIII lines at 3.476 keV and 3.515 keV separately in the spectral fit, but since the two normalizations are not independent, we sum them here.

In principle, the expected flux of K XVIII can be calculated based on the ratio of the emissivity of the K XVIII lines to these strong lines and the measured strong line fluxes. However, the relative emissivities of different lines is a sensitive function of the plasma temperature. In addition, the relative fluxes of lines of different elements depend on their relative abundances in the medium. We nominally assume that the relative elemental abundances track their ratios in the Sun Anders & Grevesse (1989), though variation in the relative abundances by a factor of 2-3 would not be unreasonable (e.g. Muno et al. 2004; Heard & Warwick 2013a; Uchiyama et al. 2013).

Thermal emission from the Galactic center region is multi-temperature and is typically modeled as having contributions from both low temperature, $kT \sim 0.8 - 1$ keV, and high-temperature, $kT \sim 6 - 8$ keV, components (e.g. Muno et al. 2004; Heard & Warwick 2013b,a; Uchiyama et al. 2013), though the high-temperature component may alternately stem from unresolved point sources (see e.g. Wang et al. 2002; Revnivtsev et al. 2009;

Heard & Warwick 2013a). Additional thermal components are contributed by individual sources in the region, including the Sagittarius A East supernova remnant (e.g. Park et al. 2005; Koyama et al. 2007) and the Arches massive star cluster (Wang et al. 2006; Tsujimoto et al. 2007).

Line emissivities for a given assumed temperature are taken from AtomDB (Smith et al. 2001). Given the clear multiphase nature of this region, we consider a range of possible plasma temperatures from 0.8 to 8.0 keV. Assuming the relative abundances track solar, in principle the ratios of the measured fluxes of the strong lines should give us an indication of the plasma temperature, but we found that these do not paint a consistent picture. For example, the ratio of S XVI to Ar XVII would indicate a low temperature of ~ 0.8 keV, while the Ar XVII to Ca XIX ratio points to a $kT \sim 2$ keV. The measured Ca XX flux instead implies a high temperature with the ratio of Ca XX to either Ca XIX or Ar XVII giving $kT \sim 3 - 4$ keV; however, both of the Ca line fluxes are too high compared to the measured S XVI flux for any temperature. Note that at temperatures less than about 2 keV the emission near 4.1 keV is expected to have significant contributions from Ar XVII and to a lesser extent K XVIII, while for temperatures greater than 2 keV, Ca XX emission dominates. When calculating the predicted line strength we sum all important contributions for a given temperature. In general, the measured flux of the line at 4.1 keV is higher than would be expected for a low-temperature plasma, even including possible Ar XVII and K XVIII contributions. Finally, the ratio of the emissivity of Ar XVII at 3.13 keV to Ar XVII at 3.69 keV is fixed (i.e. not temperature dependent) and expected to be 9.4; the measured ratio is 6.3 for MOS and 5.1 for PN. The above discussion gives an indication of the rather large systematic uncertainties present in both the modeling and the measurements which effect the ability to distinguish plasma line emission from potential dark matter line emission.

In Table 3, we present predictions for the expected flux of K XVIII (3.476+3.515 keV) based on the measured fluxes of the listed five strong lines and on the relative line emissivities for several assumed temperatures bounding those measured for the diffuse plasma near the Galactic center and the temperatures implied by the flux ratios of our strong lines; separate predictions are made for the MOS and PN instruments. For $kT = 5.0$ keV, we also include the expected contribution of Cl XVII at 3.51 keV to expected line

Line	Energy keV	MOS Flux photons cm ⁻² s ⁻¹	PN Flux photons cm ⁻² s ⁻¹
S XVI	2.62	1.4e-4	1.3e-4
Ar XVII	3.13	2.9e-4	3.0e-4
Ar XVII	3.69	4.6e-5	5.9e-5
Ca XIX	3.90	1.9e-4	1.9e-4
Ca XX	4.1	3.8e-5	4.0e-5
K XVIII	3.5	4.1e-5	2.8e-5

Table 2. Measured fluxes of the most prominent plasma lines between 2.6 and 4.5 keV in the Galactic center. Fluxes are listed separately for the combined MOS and PN spectra. Also listed is the summed flux of detected line emission at 3.48 and 3.52 keV, the position of plasma lines from K XVIII.

Predicted MOS K XVIII Flux					
kT	S XVI	Ar XVII (3.13 keV)	Ar XVII (3.69 keV)	Ca XIX	Ca XX/Ar XVII/K XVIII
0.8	5.0e-6	3.5e-6	5.4e-6	2.1e-5	4.4e-5
1.0	3.1e-6	4.3e-6	6.6e-6	2.3e-5	5.2e-5
2.0	1.5e-6	7.7e-6	1.2e-5	1.4e-5	3.9e-5
5.0	1.1e-6	2.0e-5	3.0e-5	1.1e-5	4.1e-6
Predicted PN K XVIII Flux					
kT	S XVI	Ar XVII (3.13 keV)	Ar XVII (3.69 keV)	Ca XIX	Ca XX/Ar XVII/K XVIII
0.8	4.5e-6	3.7e-6	6.8e-6	2.2e-5	4.6e-5
1.0	2.9e-6	4.5e-6	8.2e-6	2.4e-5	5.4e-5
2.0	1.4e-6	8.0e-6	1.4e-5	1.4e-5	4.1e-5
5.0	9.7e-7	2.1e-5	3.8e-5	1.2e-5	4.3e-6

Table 3. Predicted flux of the combined K XVIII lines at 3.48 and 3.52 keV based on the measured fluxes of several strong plasma emission lines and for a range of assumed plasma temperatures. For a plasma temperature of 5.0 keV, Cl XVII emission at 3.51 keV also contributes, and we include this emission in our predictions. For the measured line emission at 4.1 keV we include contributions from Ca XX, Ar XVII, and K XVIII; Ca XX dominates at temperatures above 2 keV, and Ar XVII for temperatures below 2 keV.

flux near 3.5 keV. For a given assumed temperature the predictions for the K XVIII flux vary by an order of magnitude, depending on which line is used to make the prediction; for all temperatures (0.8–5 keV), the measured K XVIII flux (Table 2) is within the predicted range, particularly given possible abundance variations between elements. We, therefore, find *no indications of line emission near 3.5 keV in excess of what expected from known astrophysical plasma lines*. While taking a lower limit on the predicted K XVIII flux would allow for potential dark matter emission, we do not consider this to be the most natural origin of the observed flux at 3.5 keV.

2.3 Implications for Dark Matter Decay

In this section we describe the implications for dark matter decay of the *XMM* observations analyzed above. We obtain three different results:

(i) a *conservative* constraint on the maximal dark matter lifetime for a dark matter particle decaying to a two-body final state including a photon of 3.5 keV energy, from a 2-sigma upper limit to the total X-ray flux at 3.5 keV from *XMM* MOS and PN observations;

(ii) an *optimized* constraint, where we take the best-fit model with the measured line flux from the K XVIII lines and find the 2-sigma upper limit on the flux of an additional line at 3.57 keV (the value preferred by the cluster analysis of Bulbul et al. 2014);

(iii) a model where we limit the K XVIII line flux to an intermediate value of 1.0×10^5 , from the range predicted in Table 3, and find the putative lifetime associated with a dark matter particle responsible for the best-fit “excess” flux above this value.

We improve here the calculation of the similar constraints obtained by Riemer-Sorensen (2014) by considering the effective integrated line-of-sight integral of the dark matter density over the relevant angular region times the actual masks employed in the observations. Co-added images of the masks used in the MOS and PN spectral extraction are shown in Fig. 2, which shows the area lost due to point source exclusion and instrumental features as well as due to the positional offset between different observations. For reference, we utilize two dark matter density profiles identical to those used in Riemer-Sorensen (2014), to which we refer the Reader for further details, namely a Navarro-Frenk and White (NFW), and an Einasto profile (EIN) with $\alpha = 0.17$, both with scale radius $r_s = 21$ kpc and a local dark matter density of 0.4 GeV/cm^3 . In addition, to obtain an even more conservative estimate of the dark matter “column density”, we also employ a Burkert (BUR) profile, with a scale radius of 6 kpc and an identical local dark matter density (it is trivial to rescale our results for a different local dark matter density). We calculate the effective *J*-factors in the direction of the Galactic center as follows

$$J \equiv \int_{\Delta\Omega} \int_{l.o.s.} A(\psi) \rho(\psi, l) dl d\Omega(\psi), \quad (2)$$

with $0 \leq A(\psi) \leq 1$ the mask profile averaged over an annulus at an angle ψ around the Galactic center, and with an angular aperture $\Delta\Omega$ roughly corresponding to the *XMM* field of view, i.e. a half-aperture angle of about 15 arcmin. We found the following effective *J* values, in units of $10^{18} \text{ GeV cm}^{-2}$ (the numbers in parenthesis

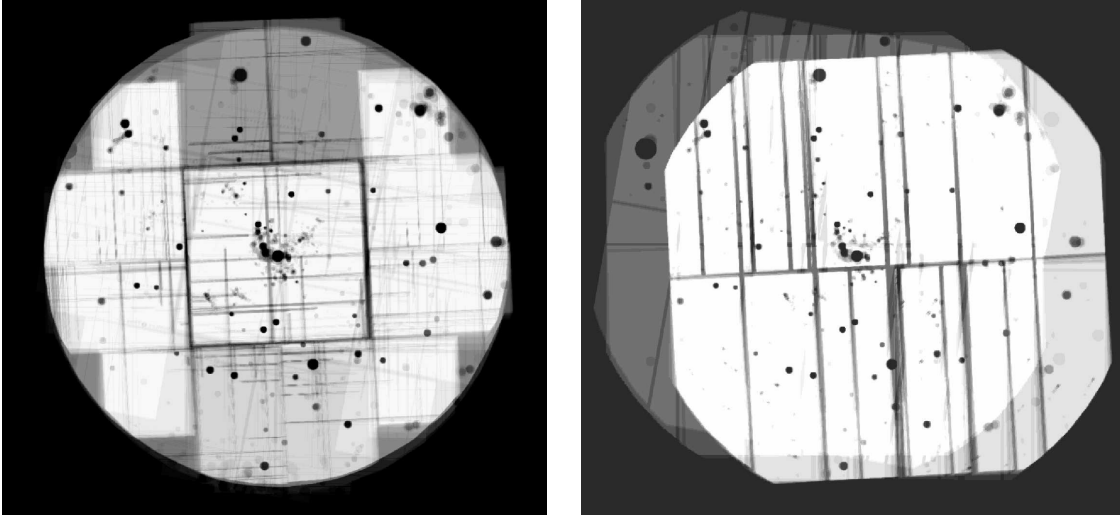


Figure 2. Co-added images of the masks used in the MOS and PN spectral extraction produced by the ESAS task *cheese*. Lost area due to point source exclusion and instrumental features are clear. These summed masks are used to correct for the effective dark matter mass probed as a function of radius.

neglect the efficiency factor, i.e. assume $A(\psi) = 1$):

$$\begin{aligned} \text{PN : } J_{\text{BUR}} &= 3.91 \text{ (5.04); } J_{\text{NFW}} = 12.5 \text{ (16.1); } J_{\text{EIN}} = 14.9 \text{ (19.2);} \\ \text{MOS : } J_{\text{BUR}} &= 3.77 \text{ (5.04); } J_{\text{NFW}} = 12.2 \text{ (16.1); } J_{\text{EIN}} = 14.4 \text{ (19.2).} \end{aligned}$$

(i) The *conservative* upper limit corresponds to the maximal flux at 2-sigma of a line near 3.5 keV, which we find to be 4.1×10^{-5} photons $\text{cm}^{-2} \text{s}^{-1}$ for MOS and 3.2×10^{-5} photons $\text{cm}^{-2} \text{s}^{-1}$ for PN. The resulting upper limits on the inverse dark matter lifetime (i.e. on the decay width $\Gamma = 1/\tau$) are as follows, in units of 10^{-28}s^{-1} :

$$\begin{aligned} \text{PN : BUR} &= 7.36; \text{NFW} = 2.28; \text{EIN} = 1.91 \\ \text{MOS : BUR} &= 9.76; \text{NFW} = 2.99; \text{EIN} = 2.54 \end{aligned}$$

(ii) The *optimized* limits, which do include the best-fit value for the K XVIII line emission at 3.5 keV, give a 2-sigma upper limit to an additional line at 3.57 keV of 2.2×10^{-6} photons $\text{cm}^{-2} \text{s}^{-1}$ for MOS and of 4.0×10^{-6} photons $\text{cm}^{-2} \text{s}^{-1}$ for PN. The resulting constraints on the dark matter inverse lifetime are as follows (again, in units of 10^{-28}s^{-1}):

$$\begin{aligned} \text{PN : BUR} &= 0.92; \text{NFW} = 0.28; \text{EIN} = 0.23; \\ \text{MOS : BUR} &= 0.52; \text{NFW} = 0.16; \text{EIN} = 0.13. \end{aligned}$$

It is worth noticing that for the most conservative choice of dark matter density profile, our optimized limits translate (via Eq. (1) above) into a 2-sigma limit on the sterile neutrino mixing angle, for a 7 keV mass, of $\sin^2(2\theta) < 2.0 \times 10^{-11}$, which excludes the best-fit value from Bulbul et al. (2014) of $\sin^2(2\theta) \sim 7 \times 10^{-11}$ and is in tension with the range of values indicated by the analysis of Boyarsky et al. (2014), i.e. $\sin^2(2\theta) \sim 2 - 20 \times 10^{-11}$; for an Einasto profile our limit of $\sin^2(2\theta) < 0.58 \times 10^{-11}$ firmly excludes the preferred ranges quoted in Bulbul et al. (2014) and Boyarsky et al. (2014) (an identical conclusion stems from using an NFW profile). For identical dark matter density profiles, our results improve by more than a factor of 2 the limits presented in Riemer-Sorensen (2014) from *Chandra* data.

(iii) Finally, the best-fit line-emissivity for a line near 3.5 keV when setting the emissivity of the K XVIII to the intermediate level

specified above is at the level of 2.1×10^{-5} photons $\text{cm}^{-2} \text{s}^{-1}$ for MOS and of 1.5×10^{-5} photons $\text{cm}^{-2} \text{s}^{-1}$ for PN. The resulting preferred range for the sterile neutrino mixing angle is, for PN, $\sin^2(2\theta) \sim 3 - 15 \times 10^{-11}$ (the lower number corresponding to an EIN profile, the higher number to the BUR case) and for MOS of $\sin^2(2\theta) \sim 5 - 21 \times 10^{-11}$. It is intriguing that these ranges align well with what Boyarsky et al. (2014) inferred for the case of M 31, though as shown below, in our own analysis we do not find any evidence for a line in M 31 at more than 1-sigma significance, and the inferred upper limit on the line flux is significantly lower than that found by Boyarsky et al. (2014).

3 COMPARISON TO CLUSTERS AND M 31

In this section, we reconsider the evidence for excess line emission near 3.5 keV in other systems, namely clusters and M 31, in light of systematic uncertainties associated with the emission strength of the K XVIII and Cl XVII lines.

3.1 Perseus and Other Clusters

Bulbul et al. (2014) present evidence of excess line emission around 3.55 to 3.57 keV from the stacked *XMM* spectra of 73 clusters of galaxies as well as individually from Perseus and a stack of Centaurus+Ophiuchus+Coma. They also analyze *Chandra* observations of the Virgo cluster but do not find excess line emission from this cluster. Bulbul et al. (2014) predict the expected K XVIII line fluxes based on the measured fluxes of S XVI (2.62 keV), Ca XIX (3.9 keV), and Ca XX (4.1 keV). In their analysis, they fit a multi-temperature thermal plasma model (using a line-free *apec* model in *XSPEC*) with 2-4 thermal components. The expected flux of the K XVIII lines is then calculated as a sum over the expectations for the different fit temperatures weighted by the relative normalizations of the individual thermal components from the spectral fit. They then take a central value from the range of predicted K XVIII fluxes given the three strong lines used as predictors; in their spectral fits they then allow the K XVIII line normalizations to go a factor of

three above this prediction to account for potential abundance variation. They conclude that the excess emission detected is a factor of 10-20 larger than the K XVIII flux predicted in this way.

While this is an entirely reasonable procedure, it may not capture the true thermal complexity of a cool-core system with AGN feedback like Perseus, nor of a stack of 73 clusters each with their own different intracluster medium structure. In fact, the temperatures derived even from the multi-temperature fit do not agree for the same objects observed with different instruments (e.g. Perseus for *XMM* MOS versus Perseus for *XMM* PN, see Bulbul et al. 2014, Table 2), which leads to differing predictions for K XVIII. As we have seen from our Galactic center analysis, different strong lines also do not give consistent predictions for the strength of K XVIII. Here we study whether, under reasonable assumptions, the expected K XVIII line fluxes in clusters might be higher than what quoted in Bulbul et al. (2014), based on the quoted line strengths for S XVI, Ca XIX, and Ca XX in Tables 2 and 7 of their paper, and including the Cl XVII line, which was neglected in Bulbul et al. (2014).

First we consider the measured fluxes for S XVI, Ca XIX, and Ca XX and what their ratios imply for the thermal state in clusters. While the exact ratio depends on the sample and instrument considered, the Ca XIX to S XVI ratio for clusters tends to be on the range 0.2-0.5. This ratio would imply a *very low* temperature plasma with $kT < 1$ keV. On the other hand, the Ca XX to S XVI ratio for clusters is measured to be in the range 0.1-0.3, which would require a *very high* temperature plasma in excess of 9 keV. Finally, the Ca XX to Ca XIX ratio for clusters is in the range 0.4-1.0, which would place the temperature in the “*intermediate*” 4-7 keV range. In fact, this pattern of line fluxes is similar to the one seen in the Galactic center, with the S XVI flux being relatively low compared to other strong lines and the Ca XX flux being relatively high compared to other strong lines. Lacking additional information, what this implies for the flux of K XVIII or other plasma lines near 3.5 keV is unclear.

Though the strong lines themselves do not paint a consistent picture, we now consider what the predicted flux of K XVIII plus Cl XVII would be for a range of plasma temperatures and compare this to the measured “excess” line flux as listed in Table 5 of Bulbul et al. (2014) both for the stacked cluster samples and the individual fits to the Perseus cluster. For the Perseus cluster, Bulbul et al. (2014) analyze *XMM* MOS, *XMM* PN, Chandra ACIS-I, and Chandra ACIS-S data. They do not detect excess line emission for *XMM* PN, but for the other detectors they find line emission at the level of $1 - 2 \times 10^{-5}$ photons $\text{cm}^{-2} \text{s}^{-1}$. Considering the Ca XIX line, which gives intermediate results, as a predictor of the expected K XVIII plus Cl XVII flux, we find that the flux of these lines is expected to be in excess of, or within a factor of two of the flux measured for the “unidentified” line by Bulbul et al. (2014) for plasma temperatures between 1-10 keV (the full range we considered). Similarly, using the measured Ca XX flux as a predictor would give a K XVIII flux well in excess of the unidentified line in Perseus for low temperatures and a K XVIII plus Cl XVII flux within a factor of two up to $kT \sim 8$ keV. The only strong line which would predict the plasma lines near 3.5 keV to be significantly below the flux of the measured excess is S XVI, which predicts these lines to be a factor of 4-10 less than what is seen, and which, as previously observed, seems to have a low flux compared to other strong lines. Note that in Bulbul et al. (2014) with the exception of ACIS-S, the unidentified line energy is fixed in the spectral fit to 3.56 or 3.57 keV, as derived from the full cluster MOS stack and the Perseus ACIS-S fit. This energy is somewhat offset

from the line energies of K XVIII and Cl XVII, but (a) the fit energy is uncertain at the level of 20-30 eV, and (b) given the ~ 100 eV spectral resolution the normalization of this feature is certainly not independent of the plasma line fluxes. We, therefore, consider that allowing a higher flux for K XVIII (plus Cl XVII, which was not included by Bulbul et al. (2014)) would absorb most if not all of the already low-significance excess line emission in Perseus.

The results are essentially the same for the stacked analysis of Coma+Centaurus+Ophiuchus from Bulbul et al. (2014) with both the measured Ca XIX and Ca XX fluxes predicting plasma line emission from K XVIII and Cl XVII similar in flux to the claimed excess emission over a large range in plasma temperature from 1-8 keV. For both the full stacked cluster sample and the cluster stack excluding nearby clusters, the detected excess is also similar to the predicted flux from known lines for low and high temperatures but somewhat in excess (by a factor of 3-7) for moderate temperatures near ~ 5 keV. Again, only the measured S XVI flux would imply a flux from known lines significantly less than what is measured, and even S XVI implies an excess that is typically less than a factor of 10 except at $kT > 8$ keV.

We conclude that within the systematic uncertainty in the expected flux from known plasma lines and considering additional uncertainty due to potential variation in the abundances of different elements, no conclusive excess line emission is present in the samples of clusters studied in Bulbul et al. (2014).

3.2 A Reanalysis of the *XMM* Data for M 31

Boyarsky et al. (2014) report the detection of an unidentified line in both the Andromeda Galaxy (M 31) and in a separate analysis of the Perseus Cluster. Boyarsky et al. (2014) do not report line fluxes for the astrophysical plasma lines included in their analysis. To assess the significance of possible line emission in M 31, we therefore reanalyzed the relevant archival *XMM* data. In particular, we analyzed the same M 31 data set employed by Boyarsky et al. (2014), namely the EPIC MOS data for the observations listed in their Table 3 which were determined to have low levels of contamination from particle background flares. Here, we consider only the 29 *XMM* pointings within $2'$ of the center of M 31. Data reduction and spectral stacking followed the same methodology employed for the Galactic center analysis described in Section 2.1.

Just as in the case of the Galactic center, the X-ray emission from M 31 is a complicated combination of sources, dominated by unresolved X-ray binaries and stellar sources in addition to thermal emission from a soft ~ 0.3 keV plasma (Takahashi et al. 2004; Bogdán & Gilfanov 2008; Liu et al. 2010). As with the Galactic center analysis, we concentrate on obtaining a good fit to the continuum emission near 3.5 keV rather than on modeling in detail the contributions from each of these sources. For the low average plasma temperature indicated, no strong line emission is expected in M 31 in the 3-4 keV range, nor is any evident. As shown in the left panel of Fig. 3, we find that the M 31 data are well fit by a simple power law between 3 and 4 keV, with a reduced χ^2 of 1.12 ($\chi^2 = 220.6/197$ degrees of freedom) for the combined MOS spectrum.

No significant residuals are evident in the fit, but we test for the existence of excess line emission by adding a Gaussian line with an energy allowed to vary between 3 to 4 keV. We find that the addition of a line does not significantly improve the fit, producing a reduced χ^2 of 1.11 ($\chi^2 = 216.0/195$ degrees of freedom). While the best-fit line energy is 3.53 keV, as found by Boyarsky et al. (2014), the energy is essentially unconstrained and the line normalization is not

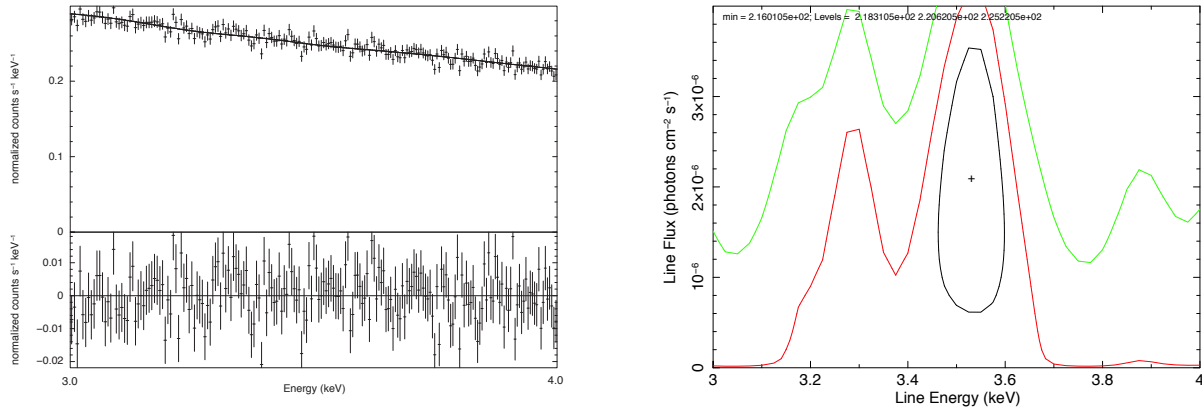


Figure 3. Left: Stacked MOS spectrum of M 31 in the 3.0 to 4.0 keV range along with the best-fit simple power law and residuals. Right: Confidence contours on the combination of line energy and line flux after a Gaussian line is added to the spectrum on the left. Contours show the 68% (black), 90% (red), and 99% (green) confidence regions.

significantly non-zero. To illustrate this important point, the right panel of Fig. 3 shows confidence contours for the line energy and flux with contours indicating the 68% (black), 90% (red), and 99% (green) confidence regions. As can be seen from this figure, the line is only present at about the 1-sigma level and the normalization is consistent with zero with the 90% confidence region. The best-fit flux we derive is also a factor of two lower than what was found by Boyarsky et al. (2014) whose flux may have been amplified by residuals in the spectrum outside of the 3–4 keV range. We conclude that *no significant line emission near 3.5 keV is detected in M 31*.

4 DISCUSSION AND CONCLUSIONS

Reports of the detection of a 3.5 keV line from observations of clusters of galaxies and of M 31 (Bulbul et al. 2014; Boyarsky et al. 2014) with no identified astrophysical line emission counterparts have triggered significant excitement, and considerable work on constructing dark matter particle models that could explain the emission. No evidence for such an excess line was subsequently found in the analysis of *Chandra* data from the center of the Galaxy reported in Riemer-Sørensen (2014), which also implied limits on a simple dark matter decay interpretation in tension with the preferred values inferred from clusters and from M31.

In this study, we analyzed *XMM* archival data from the Galactic center, with an effective total exposure about a factor 3 larger than the previous *Chandra* analysis. We also carefully assessed the expected emissivity of astrophysical lines that could produce the observed 3.5 keV feature, specifically associated with Potassium and Chlorine atomic transitions.

We obtained an excellent fit to the *XMM* data in the energy range between 3.0 and 4.5 keV by adding relevant plasma lines, including in particular two K XVIII lines at 3.48 and 3.52 keV fully explaining the observed 3.5 keV feature. Using the measured flux of brighter lines, we estimated a reasonable range for the flux of the K XVIII lines, and we found that the level of emission needed to fit the *XMM* data falls squarely within the expected range. We thus found no indications of line emission near 3.5 keV in excess of what is expected from known astrophysical plasma lines.

We produced limits on the dark matter lifetime from our *XMM*

data analysis, and showed that utilizing the best-fit value for the K XVIII lines we rule out a dark matter decay origin for both the clusters and the M 31 observations. Our limits improve previous constraints from *Chandra* observations of the Galactic center (Riemer-Sørensen 2014) by more than a factor 2. For standard dark matter density profiles (NFW or Einasto), our limits are in significant tension with the dark matter decay interpretation of the 3.5 keV lines reported in Bulbul et al. (2014) and Boyarsky et al. (2014).

We then re-examined the possible role of Potassium and Chlorine lines in the cluster analysis of Bulbul et al. (2014), and found that inferring the flux of those lines from other measured lines, and for a reasonable range of temperatures, the 3.5 keV line can be naturally explained. Finally, we re-analyzed *XMM* data from M 31, and showed that, in the relevant energy range, the spectrum is well fit by a featureless power law. We found no preference for a line at statistical significance greater than one sigma. The one-sigma excess we do find at energies around 3.5 keV also possesses a flux lower by about a factor of two compared to what claimed in Boyarsky et al. (2014).

In conclusion, while we do find evidence for a 3.5 keV line in X-ray data from the Galactic center, we showed that, within the systematic uncertainty in the expected flux from known plasma lines and considering additional uncertainty due to potential variation in the abundances of different elements, no conclusive excess line emission is present either from the Milky Way center or from clusters; also, no evidence was found of any statistically significant line from M 31 in the energy range of interest.

ACKNOWLEDGMENTS

We thank A. Boyarsky, A. Foster, and E. Storm for helpful discussions. SP is partly supported by the US Department of Energy, Contract DE-SC0010107-001.

REFERENCES

- Abada A., Arcadi G., Lucente M., 2014, 1406.6556
- Abazajian K. N., 2014, Phys.Rev.Lett., 112, 161303, 1403.0954

- Allahverdi R., Dutta B., Gao Y., 2014, 1403.5717
- Anders E., Grevesse N., 1989, *Geochimica et Cosmochimica Acta*, 53, 197, ADS
- Arnaud K. A., 1996, in Jacoby G. H., Barnes J., eds, *Astronomical Data Analysis Software and Systems V* Vol. 101 of *Astronomical Society of the Pacific Conference Series*, XSPEC: The First Ten Years. p. 17, ADS
- Baek S., Ko P., Park W.-I., 2014, 1405.3730
- Baek S., Okada H., 2014, 1403.1710
- Baer H., Choi K.-Y., Kim J. E., Roszkowski L., 2014, 1407.0017
- Blackburn J. K., 1995, in Shaw R. A., Payne H. E., Hayes J. J. E., eds, *Astronomical Data Analysis Software and Systems IV* Vol. 77 of *Astronomical Society of the Pacific Conference Series*, FTOOLS: A FITS Data Processing and Analysis Software Package. p. 367, ADS
- Bogdán Á., Gilfanov M., 2008, *MNRAS*, 388, 56, 0803.0063, ADS
- Bomark N. E., Roszkowski L., 2014, 1403.6503
- Boyarsky A., Ruchayskiy O., Iakubovskiy D., Franse J., 2014, 1402.4119
- Boyarsky A., Ruchayskiy O., Shaposhnikov M., 2009, *Ann.Rev.Nucl.Part.Sci.*, 59, 191, 0901.0011
- Bulbul E., Markevitch M., Foster A., Smith R. K., Loewenstein M., et al., 2014, 1402.2301
- Chiang C.-W., Yamada T., 2014, 1407.0460
- Choi K.-Y., Seto O., 2014, 1403.1782
- Cicoli M., Conlon J. P., Marsh M. C. D., Rummel M., 2014, 1403.2370
- Cline J. M., Farzan Y., Liu Z., Moore G. D., Xue W., 2014, 1404.3729
- Cline J. M., Frey A. R., 2014, 1408.0233
- Conlon J. P., Day F. V., 2014, 1404.7741
- Conlon J. P., Powell A. J., 2014, 1406.5518
- Demidov S., Gorbunov D., 2014, 1404.1339
- Dias A., Machado A., Nishi C., Ringwald A., Vaudrevange P., 2014, 1403.5760
- Dudas E., Heurtier L., Mambrini Y., 2014, 1404.1927
- Dutta B., Gogoladze I., Khalid R., Shafi Q., 2014, 1407.0863
- Finkbeiner D. P., Weiner N., 2014, 1402.6671
- Frandsen M. T., Sannino F., Shoemaker I. M., Svendsen O., 2014, *JCAP*, 1405, 033, 1403.1570
- Geng C.-Q., Huang D., Tsai L.-H., 2014, 1406.6481
- Haba N., Ishida H., Takahashi R., 2014, 1407.6827
- Heard V., Warwick R. S., 2013a, *MNRAS*, 428, 3462, 1210.6808, ADS
- Heard V., Warwick R. S., 2013b, *MNRAS*, 434, 1339, 1306.4186, ADS
- Higaki T., Jeong K. S., Takahashi F., 2014, *Phys.Lett.*, B733, 25, 1402.6965
- Ishida H., Jeong K. S., Takahashi F., 2014, *Phys.Lett.*, B732, 196, 1402.5837
- Jaekel J., Redondo J., Ringwald A., 2014, *Phys.Rev.*, D89, 103511, 1402.7335
- Kolda C., Unwin J., 2014, 1403.5580
- Kong K., Park J.-C., Park S. C., 2014, *Phys.Lett.*, B733, 217, 1403.1536
- Koyama K., Uchiyama H., Hyodo Y., Matsumoto H., Tsuru T. G., Ozaki M., Maeda Y., Murakami H., 2007, *Publications of the Astronomical Society of Japan*, 59, 237, ADS
- Krall R., Reece M., Roxlo T., 2014, 1403.1240
- Kuntz K. D., Snowden S. L., 2008, *Astronomy & Astrophysics*, 478, 575
- Lee H. M., 2014, 1404.5446
- Lee H. M., Park S. C., Park W.-I., 2014, 1403.0865
- Liew S. P., 2014, *JCAP*, 05, 044, 1403.6621
- Liu J., Wang Q. D., Li Z., Peterson J. R., 2010, *MNRAS*, 404, 1879, 1001.4058, ADS
- Modak K. P., 2014, 1404.3676
- Muno M. P., Baganoff F. K., Bautz M. W., Feigelson E. D., Garmire G. P., Morris M. R., Park S., Ricker G. R., Townsley L. K., 2004, *Astrophys.J.*, 613, 326, astro-ph/0402087, ADS
- Nakayama K., Takahashi F., Yanagida T. T., 2014, 1403.1733
- Nowak M. A., Neilsen J., Markoff S. B., Baganoff F. K., Porquet D., Grosso N., Levin Y., Houck J., Eckart A., Falcke H., Ji L., Miller J. M., Wang Q. D., 2012, *Astrophys.J.*, 759, 95, 1209.6354, ADS
- Okada H., 2014, 1404.0280
- Okada H., Orikasa Y., 2014, 1407.2543
- Okada H., Toma T., 2014, 1404.4795
- Pal P. B., Wolfenstein L., 1982, *Phys.Rev.*, D25, 766
- Park S., Muno M. P., Baganoff F. K., Maeda Y., Morris M., Charatas G., Sanwal D., Burrows D. N., Garmire G. P., 2005, *Astrophys.J.*, 631, 964, astro-ph/0506168, ADS
- Queiroz F. S., Sinha K., 2014, 1404.1400
- Revnivtsev M., Sazonov S., Churazov E., Forman W., Vikhlinin A., Sunyaev R., 2009, *Nature*, 458, 1142, 0904.4649, ADS
- Riemer-Sorensen S., 2014, 1405.7943
- Ringwald A., 2014, 1407.0546
- Robinson D. J., Tsai Y., 2014, 1404.7118
- Rodejohann W., Zhang H., 2014, 1407.2739
- Rosner J. L., 2014, 1404.5198
- Shuve B., Yavin I., 2014, 1403.2727
- Smith R. K., Brickhouse N. S., Liedahl D. A., Raymond J. C., 2001, *ApJ Letters*, 556, L91, astro-ph/0106478, ADS
- Snowden S. L., Mushotzky R. F., Kuntz K. D., Davis D. S., 2008, *Astronomy & Astrophysics*, 478, 615, 0710.2241
- Takahashi H., Okada Y., Kokubun M., Makishima K., 2004, *Astrophys.J.*, 615, 242, astro-ph/0408305, ADS
- Tsujimoto M., Hyodo Y., Koyama K., 2007, *Publications of the Astronomical Society of Japan*, 59, 229, astro-ph/0611104, ADS
- Tsuyuki T., 2014, 1403.5053
- Uchiyama H., Nobukawa M., Tsuru T. G., Koyama K., 2013, *Publications of the Astronomical Society of Japan*, 65, 19, 1209.0067, ADS
- Wang Q. D., Dong H., Lang C., 2006, *MNRAS*, 371, 38, astro-ph/0606282, ADS
- Wang Q. D., Gotthelf E. V., Lang C. C., 2002, *Nature*, 415, 148, ADS